Numerical Heat Transfer, Part A: Applications: An International Journal of Computation and Methodology

Publication details, including instructions for authors and subscription information:
http://www.tandfonline.com/loi/unht20

Effects of Roughness of Gas Diffusion Layer Surface on Liquid Water Transport in Micro Gas Channels of a Proton Exchange Membrane Fuel Cell

Li Chen [a], HuiBao Luan [a], Ya-Ling He [a] & Wen-Quan Tao [a]

[a] Key Laboratory of Thermo-Fluid Science and Engineering of MOE, School of Energy and Power Engineering, Xi'an Jiaotong University, Xi'an, Shaanxi, P.R. China

Version of record first published: 02 Aug 2012

To cite this article: Li Chen, HuiBao Luan, Ya-Ling He & Wen-Quan Tao (2012): Effects of Roughness of Gas Diffusion Layer Surface on Liquid Water Transport in Micro Gas Channels of a Proton Exchange Membrane Fuel Cell, Numerical Heat Transfer, Part A: Applications: An International Journal of Computation and Methodology, 62:4, 295-318

To link to this article: http://dx.doi.org/10.1080/10407782.2012.670586

Numerical Heat Transfer, Part A, 62: 295–318, 2012

ISSN: 1040-7782 print/1521-0634 online
DOI: 10.1080/10407782.2012.670586

Taylor & Francis
Taylor & Francis Group

EFFECTS OF ROUGHNESS OF GAS DIFFUSION LAYER SURFACE ON LIQUID WATER TRANSPORT IN MICRO GAS CHANNELS OF A PROTON EXCHANGE MEMBRANE FUEL CELL

Li Chen, HuiBao Luan, Ya-Ling He, and Wen-Quan Tao
Key Laboratory of Thermo-Fluid Science and Engineering of MOE, School of Energy and Power Engineering, Xi'an Jiaotong University, Xi'an, Shaanxi, P.R. China

Effects of surface roughness of a gas diffusion layer (GDL) on liquid water transport in a micro gas channel (GC) of a proton exchange membrane fuel cell (PEMFC) are investigated by using the volume of fluid (VOF) method in the commercial CFD package, FLUENT 6.3.26. An array of cubic holes under the GDL surface is used to describe the GDL surface roughness. The simulation results show that a Cassie droplet is inclined to form on the hydrophobic rough GDL surface and the surface roughness greatly affects the transport of the droplet. Effects of GDL surface roughness on forces acting on the droplet are carefully studied, and it is found that GDL surface roughness reduces the retentive forces and increases the detaching forces. In addition, effects of GDL surface roughness on the time required for a droplet to be removed out of the GC, liquid water coverage area ratio on GDL surface, and pressure drop in the GC are explored. The removal time of the water droplet decreases as the GDL roughness increases. The water coverage ratio of the GDL surface decreases as GDL surface roughness increases. The pressure drop in the GC increases as the GDL surface roughness increases.

1. INTRODUCTION

The proton exchange membrane fuel cell (PEMFC) is a promising candidate of power source for a range of applications because of its notable advantages such as high power density, high efficiency, low operation temperature, low noise, and no pollutions. However, PEMFC requires further improvements to achieve wide commercial use, particularly in regard to cell performance. To improve performance of PEMFC, proper water managements are urgently demanded. Successful water management in the PEMFC, particularly in the cathode side, is crucial to the cell performance, as poor water management results in either dehydration of the membrane or flooding issues. On the one hand, membrane dehydration increases the

Received 22 July 2011; accepted 13 February 2012.
The authors thank the National Nature Science Foundation of China (no. 51136004) for supporting this work.
Address correspondence to Wen-Quan Tao, Key Laboratory of Thermo-Fluid Science and Engineering of MOE, School of Energy and Power Engineering, Xi'an Jiaotong University, Xi'an, Shaanxi 710049, P.R. China. E-mail: wqtao@mail.xjtu.edu.cn

NOMENCLATURE

A_r	liquid water area fraction at the outlet of GC	l	diameter of the contact area between liquid water and the GDL surface, m
A_w	area of water at the GC outlet, m^2	n	surface normal
A_{outlet}	total area of the GC outlet, m^2	P	pressure, Pa
b	height between the top of the droplet and the top wall of the GC, m	r	radius of the emergence pore, m
C	volume fraction function	R	radius of the water droplet, m
F_{ad}	surface tension force due to interface pressure difference across the water-air interface, N	Re	Reynold number
F_b	buoyancy force, N	t	time, s
F_g	gravity force, N	u	velocity, m s^{-1}
F_l	lift force, N	V	volume of the water droplet, m^3
F_p	pressure force, N	μ	dynamic viscosity, N s m^{-2}
F_R	surface tension force due to water deformation, N	σ	surface tension between water and air, N m^{-1}
F_r	surface tension force due to water connected to the emergence pore, N	θ	contact angle
F_s	shear force, N	θ_a	advancing contact angle
g	gravity acceleration, m s^{-2}	θ_r	receding contact angle
h	the height of the liquid water droplet, m	ρ	density, kg m^{-3}
H	height of the GC, m	υ	kinematic viscosity, $m^2 s^{-1}$

Subscripts

a	air
in	inlet
w	water

proton conductive resistance and thus reduces the cell performance owing to great ohmic loss across the membrane. On the other hand, flooding problems occur if excessive liquid water accumulates in the components of a PEMFC including gas channel (GC), gas diffusion layer (GDL), and catalyst layer (CL). Flooding can seriously debilitate cell performance which concretely presents as three sub-category flooding issues. On the microscopic scale, liquid water covers the CL surface, creating hindered oxygen transport and reduced reactive surface. On the mesoscopic scale, liquid water clogs pores of GDL, decreasing the effective transport of gaseous reactant to the reactive site. On the macroscopic scale, liquid water blocks the GC, resulting in mal-distribution of oxygen and an increase in parasitic pumping power to overcome the increased pressure drop. Therefore, much research has highlighted and emphasized the requirement of proper water management and have endeavored to investigate liquid water transport processes in the components of a PEMFC. Reviews of these studies have been conducted in references [1–3].

Liquid water dynamics in the GC is one of the most important issues in the process of water management, which has been extensively studied during the past several years [3]. Liquid water transport and distribution in the GC are affected by various operating conditions: air flow rate significantly affects liquid water distribution and leads to different water flow patterns [4]; decreasing the inlet humidity of the reactants can greatly mitigate buildup of liquid water [5]; raising the operating temperature can considerably reduce the liquid water content [6]; and operating PEMFC under different loads' results in various liquid water distribution [7]. In addition, liquid water distributions in the GC are also affected by several geometrical

Table 1. Simulations of liquid water transport dynamics in the GC using the VOF method

Authors and published year	Components and GC dimensions 3-D: Height × width × length (mm) 2-D: Height × length (mm)	Research aspects
Quan et al. [17]	A U-shaped GC $1 \times 1 \times 20$ Smooth GC bottom surface without water inlet pore	Transport process of liquid water with different initial distribution
Zhan et al. [20]	Single rectangle GC $1 \times 1 \times 11.5$ Single serpentine GC $1 \times 1 \times 23$ Smooth GC bottom surface without water inlet pore	Effects of air inlet velocity and GC wall wettability on liquid water behaviors
Cai et al. [19]	Single rectangle GC $1 \times 1 \times 20$ GC Bottom surface: Smooth without water inlet pore	Effects of GC wall wettability on liquid water transport and distribution
Theodorakakos et al. [25]	A small fraction of GC Smooth GC bottom surface with water inlet pore	Effects of air velocity on the droplet detachment
Jiao et al. [18]	Three parallel GCs $1 \times 1 \times 10$ Smooth GC bottom surface without water inlet pore	Transport process of liquid water with different initial distribution
Jiao et al. [21]	Serpentine rectangle GCs $1 \times 1 \times 10$ Smooth GC bottom surface without water inlet pore	Transport process of liquid water with different initial distribution
Jiao et al. [31]	U-shaped GCs with innovative GDL $1 \times 1 \times 30$	Effects of innovative GDL structures on liquid water transport and distribution
Zhu et al [26]	Single rectangle GC (2-D) 0.25×1 Smooth GC bottom surface with water inlet pore	Effects of GC size, inlet pore size and air velocity on liquid water dynamic behaviors
Jiao et al. [32]	A U-shaped GC with innovative GDL $1 \times 1 \times 30$	Effects of GDL wettability on liquid water transport and distribution
Ebrahim and Shila [22]	Single rectangle GC (2-D) 0.125×1 without water inlet pore	Effects of gas inlet velocity, the density and viscosity of the gas, and the surface tension coefficient on the droplet deformation
Le and Zhou [33]	Whole PEMFC	3-D general model for PEMFC involving coupled process of liquid water distribution and reactant transport
Zhu et al. [27]	Single rectangle GC $0.25 \times 0.25 \times 1$ Smooth GC bottom surface with water inlet pore	Effects of inlet air velocity, GC wall wettability, water inlet velocity, and water inlet pore size on liquid water distribution
Le and Zhou [34]	Whole PEMFC	3-D general model for PEMFC involving coupled process of liquid water distribution and reactant transport
Zhu et al. [28]	Single GC with different cross-sections Smooth GC bottom surface with water inlet pore	Effects of GC cross-sections on liquid water dynamic behaviors
He et al [23]	Single rectangle GC $1.05 \times 1.05 \times 10$ Rough GC bottom surface without water inlet pore	Effects of GC bottom wall surface roughness on liquid water behaviors
Le et al. [30]	Serpentine rectangle GCs and homogenous GDL	Liquid water transport behaviors within the GDL and GC

(*Continued*)

Table 1. Continued

Authors and published year	Components and GC dimensions 3-D: Height × width × length (mm) 2-D: Height × length (mm)	Research aspects
Ding et al. [29]	Single rectangle GC $0.25 \times 0.25 \times 1.25$ Partially rough GC bottom surface with water inlet pore	Effects of water inlet pore structure, water inlet velocity, and GC wall wettability on liquid water distribution
Akhtar and Kerkhof [24]	Single tapered channel length: 20 Height × width (inlet): 1×1 Height × width (outlet): 0.5×1 Smooth GC bottom surface without water inlet pore	Effects of wall wettability on liquid water behaviors.

parameters (e.g., GC layout, GC surface wettability, and land/channel width ratio). Different layouts of GC (currently, parallel, interdigitated, and serpentine layouts are the most commonly adopted layouts) create different liquid water distribution in the GC [8]. The geometrical configuration of the channel also greatly impacts the liquid water distribution in the GC, including the cross-section of the GC [9], the channel number and the land/channel width ratio [10], and the GC surface wettability [11].

Numerical simulations have been performed to investigate the effects of various operating conditions and geometrical parameters on liquid water behaviors in the GC. A multiphase mixture model [12, 13] and multi-fluid multi-phase model [14–16] have been widely adopted in modeling two-phase flow problems. Recently, the volume of fluid (VOF) method has also been applied to explore liquid water behaviors in the GC, due to its capacity of considering surface tension and wall adhesion and of tracking liquid-gas interface [17–34]. Table 1 presents a brief introduction to those numerical studies using VOF. These studies can be divided to different groups based on different classifications. For the computational domain, some focused on the GC [17–19], some further considered the cathode of the PEMFC [30–32], and some comprehensively took the whole PEMFC into account [33, 34]. For initial liquid water distribution, some started the simulation with initial given liquid water distribution [17–24, 30, 33, 34], while others performed the simulation with liquid water gradually entering the GC from GDL pores [25–29, 31, 32]. For the GC bottom surface which consisted of GDL, some simply used a smooth bottom surface [17–29] while some tried to involve the GDL surface roughness [23, 29]. For the coupling process of liquid water and reactants transport, some concentrated on the liquid water behaviors [17–32] and some further [33, 34] simulated the coupled process of liquid water and reactant transports. Besides, the above simulations put an emphasis on different factors that affect liquid water formation and movement, e.g., gas or liquid water velocity, contact angle hysteresis, wall wettability, surface roughness, GC dimensions, cross-section shape of GC, and GC layout. The above studies have revealed that liquid water distribution in the GC is highly variable and liquid water transport in the GC is significantly complicated for its inherently unsteady and nonlinear characteristics.

In PEMFC, the GC is usually carved in the bipolar plate which is directly adjacent to the porous GDL. Therefore, three walls of a GC (the top and two side

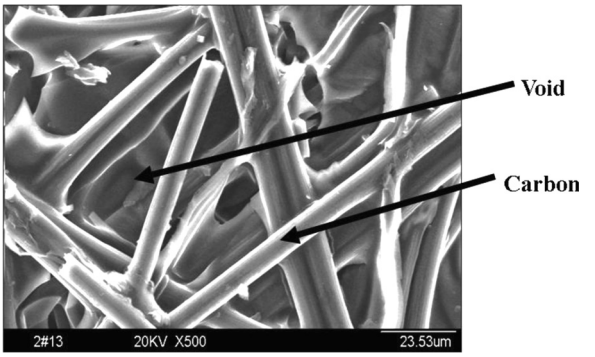

Figure 1. Microstructure of carbon paper GDL.

walls in this study) consist of bipolar plate material and the fourth wall (the bottom wall in this study) is composed of the GDL. The GDL has very complex microscopic structures. Figure 1 shows an SEM image of a carbon paper GDL. Clearly, the complex and nonuniform structures of GDL create a rough bottom surface of a GC. In a micro GC, such a rough bottom surface significantly affects liquid water transport and distribution [29]. This is because surface tension force, which plays an important role on liquid water dynamics in micro GC, is closely related to surface roughness. However, to the best of our knowledge, few studies have considered the rough surface of the GDL when studying liquid water dynamic behaviors in the GC. Only very recently, He et al. [23] distributed long rectangles on the GC bottom surface to describe GDL surface roughness, and the simulation results revealed a great impact of GDL surface roughness on liquid water transport processes. Ding et al. [29] arranged cube holes dispersed on the GDL surface and they found out that the GDL surface microstructures give rise to various liquid water flow patterns.

The objective of the present study is to investigate the effeets of GDL surface roughness on liquid water behaviors in a micro GC of a PEMFC. Emphasis is placed on the effects of roughness on forces affecting liquid water transport and the resulting pressure drop in the GC, liquid water coverage area on the GDL surface, and liquid water removal rate. The following sections are arranged. The computational domain, computational methodology, and boundary and initial conditions are introduced in section 2. In section 3, the effects of GDL surface properties on forces acting on liquid water, liquid water removal rate, liquid water coverage area on GDL surface, and pressure drop in the GC are investigated in detail. Finally, a conclusion is given in section 4.

2. NUMERICAL MODEL

2.1. Computational Domain

As mentioned above, liquid water transport processes in the GC are affected by many operating parameters and geometrical parameters. In this study, we focus on the effects of GDL surface roughness on liquid water behaviors in the GC. Therefore, all the operating conditions including air inlet velocity, operating temperature, and operating pressure are kept constant. Geometrical parameters including GC

height, GC width, and GC length also are fixed. Only the GDL surface wettability and the roughness of the GDL surface are varied during the simulations. It is worth mentioning that temperature plays an important role on cell performance. It causes evaporation or condensation between liquid water and water vapor, affects transport parameters including diffusivity and iron conductivity, and changes the electrochemical reaction rate. In the present study, emphasis is put on liquid water dynamic behaviors in the GDL and thus phase change is not considered. Neglecting phase change is a common assumption in the literature, where the focus was on liquid water transport processes [17–29]. Besides, species diffusion, iron conduction, and electrochemical reaction are also not considered in the present study. On the whole, the effects of temperature is limited and the isothermal assumption is reasonable in the present study.

Figure 2 shows the schematic of the 3-D computational domain, which is a rectangle with a square cross-section. The height of the GC is 300 μm and the length of the GC is 1000 μm. Similar to reference [27], a relatively large square pore is located at the midline of the GDL surface, which serves as the emergence pore for liquid water from the GDL. The width of the emergence pore w_1 is 60 μm and the distance between the pore and GC inlet L_1 is 200 μm.

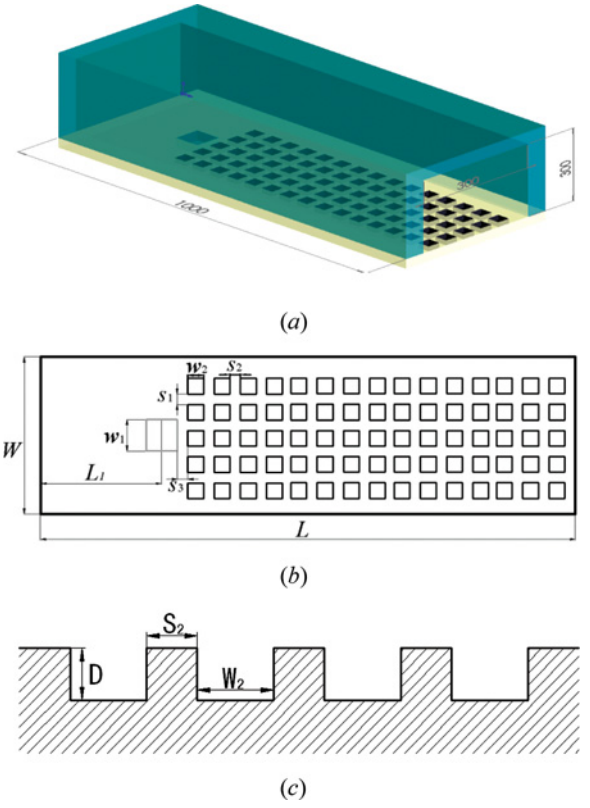

Figure 2. Computational domain. (*a*) Three-dimensional structure, (*b*) schematic of the GDL surface, and (*c*) schematic of the roughness elements (color figure available online).

In this study, the roughness of GDL surface is represented by an array of cubic holes distributed on the GDL surface, as shown in Figure 2*a*. Both the depth D and width w_1 of the cubic holes are 20 μm. Five cases with different roughness of GDL surface are considered. Different roughness is obtained by altering the gap between square holes in the flow direction (S_2 in Figure 2*b*). Obviously, a larger gap between cubic holes indicates lower roughness. The roughness (or roughness factor) of the GDL surface in the present study is defined as follows.

$$r_{\mathrm{GDL}} = 1 + 4S_2D/(S_2 + w_2)^2 \tag{1}$$

Therefore, the roughness of the GDL for different simulated cases can be quantitatively determined and is listed in Table 2. In Table 2, case 5 is the case with a smooth GDL surface and no hole is arranged on the GDL surface.

In the present studies, cubic holes are only distributed downstream the emergence pore, as this was done in reference [23]. This is because liquid water from the emergence pore can't move upstream due to the air flow from upstream. Although such treatment changes the flow field upstream in the GC, the change is believed to be slight and has little effect on liquid water dynamic behaviors in the GC. Therefore, to save computational resources, cubic holes are not arranged upstream the emergence pore.

2.2. Computational Methodology

The two-phase unsteady problems taking place in the computational domain can be briefly described as follows. Liquid water enters the GC from the emergence pore and gradually grows bigger; since liquid water is subjected to the air flow from the GC inlet, it deforms and moves towards the downstream. Due to the low Reynolds number and negligible generated heat, the unsteady two-phase flow is assumed to be isothermal laminar flow without phase change in this study.

The volume of fluid (VOF) method in the commercial CFD package, FLUENT 6.3.26 is employed to simulate the two-phase flow in the GC. An explicit VOF formulation is adopted to track the interface between the liquid water and air. The pressure-implicit with splitting of operators (PISO) scheme is used for the velocity-pressure coupling. Updating the interface location is achieved by using the piecewise linear interface calculation (PLIC) [35]. For a more detailed description of FLUENT 6.3.26 one can refer to reference [36].

Table 2. Simulation cases in this study

Case	S_1 (μm)	S_2 (μm)	r_{GDL}	Contact angle (°)
1	20	20	2	60°, 125°, 145°
2	20	40	1.88	125°, 145°
3	20	60	1.75	125°, 145°
4	20	80	1.64	125°, 145°
5	—	—	1	125°, 145°

In the VOF method, volume fraction functions C_a and C_w are defined for air and liquid water to track air-liquid water interface. The sum of C_a and C_w in a computational cell is 1.

$$C_a + C_w = 1 \tag{2}$$

The tracking of the interface is accomplished by solving the following equation in each computational cell.

$$\frac{\partial(C_w)}{\partial t} + \nabla \cdot (C_w u_w) = 0 \tag{3}$$

The governing equations are the continuity and the Navier-Stokes equations.

$$\frac{\partial(\rho)}{\partial t} + \nabla \cdot (\rho u) = 0 \tag{4}$$

$$\frac{\partial(\rho u)}{\partial t} + \nabla \cdot (\rho u u) = -\nabla p + \nabla \cdot [\mu(\nabla u + \nabla u^T)] + \rho g + F \tag{5}$$

where p is the pressure. ρ and μ are volume-averaged density and dynamic viscosity, which are calculated with linear interpolation using the volume fraction function C_k.

$$\rho = \rho_a C_a + \rho_w C_w \tag{6}$$

$$\mu = \mu_a C_a + \mu_w C_w \tag{7}$$

F in Eq. (5) is the force term due to surface tension by adopting the continuum surface force (CSF) model [37].

$$F = 2\sigma k \frac{\rho \nabla C_w}{(\rho_a + \rho_w)} \tag{8}$$

where σ is the surface tension coefficient and k is the mean curvature of the interface which is calculated as follows.

$$k = \nabla \cdot \left(\frac{\nabla C_w}{|\nabla C_w|} \right) \tag{9}$$

2.3. Boundary and Initial Conditions

At the left inlet of the GC, air velocity is fixed as $10\,\mathrm{m\,s^{-1}}$. The corresponding Re is about 160 (based on the hydraulic diameter of the channel), which is of the same order as flow encountered in automotive fuel cell stacks [38]. Besides, similar air velocity is widely used in the literature where liquid water dynamic behaviors in a micro channel was numerically investigated [23, 27, 28]. At the right exit, fully developed flow is assumed. Liquid water injection rate from the emergence pore is specified as $1\,\mathrm{m\,s^{-1}}$. For a fuel cell with current density of 1 A $\mathrm{cm^{-2}}$, it's assumed all the water generated is liquid and the liquid water generation rate is about

9.34×10^{-5} ml s^{-1} cm^{-2}. For a reactive area at 10 cm^2, the liquid water injection rate specified here is sufficient to drain all the liquid water from CL through GDL to the GC. It has been reported [27] that within a certain range of Re (50 in their study), liquid water shows similar dynamic behaviors. As dimensions of the micro channel and the emergence pore in the present study is quite similar to that in reference [27], the relatively large liquid water inlet velocity used in reference [27] is also adopted in the present study to help reduce the simulation time. Using such relatively large inlet velocity, although leads to shorter liquid water removal time, will not change the qualitative results obtained in the present study. Besides, as reported in reference [27], such a liquid water injection rate is of the same order as that used in an ex situ fuel cell experiment [39]. The surface tension coefficient between liquid water and air is set as 0.0725 N m^{-1}. A hydrophilic GC is adopted because it is beneficial for liquid water removal and reactants transport [19]. Therefore, the static contact angle is set as 45° between liquid water and two side walls, and between liquid water and the top wall. No slip boundary condition is applied to all the solid walls. The operating temperature and pressure are 330 K and 101325 Pa, respectively. The convergence criterions for all variables are set as 10^{-6}.

2.4. Mesh and Time Step

There are about 101,088 structured orthogonal meshes in the computational domain, with the meshes in the cubic holes and the emergence pore refined twice. Figure 3 shows the meshes at $x = 260\,\mu$m for case 1. The mesh independency is validated by performing simulations for case 1 with three different mesh sizes. It is found that 101,088 meshes are adequate to capture the water behaviors. Simulations with time steps of 1×10^{-7}, 5×10^{-7}, and 5×10^{-8} s are also performed for case 1, and no obvious difference is found. Therefore, the time step is set as 1×10^{-7} s in the simulation.

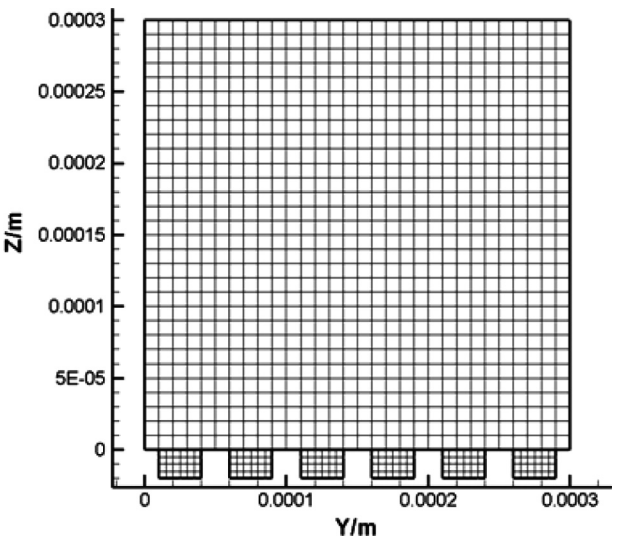

Figure 3. Mesh at $x = 260\,\mu$m for case 1.

3. RESULTS AND DISCUSSION

Water management inside GC can be optimized by reducing the liquid water coverage area on the GDL surface, increasing the removal rate of liquid water and minimizing pressure drop in the GC. Therefore, we focus on the effects of the roughness of the GDL surface on the above three parameters.

3.1. Effects of GDL Surface Wettability

Previous to investigating the effects of surface roughness, the effects of GDL surface wettability are studied. GDL surface wettability plays a significant role on liquid water behaviors in the GC. The contact angle is commonly used to quantify the wettability of a solid surface. It is defined as the angle at which the liquid/gas interface meets the solid surface. If the contact angle is less than 90°, the solid surface is hydrophilic and liquid water spreads as film. If the contact angle is greater than 90°, the solid surface is hydrophobic and liquid water forms droplets. In this section, simulations are performed for case 1 to investigate liquid water behaviors in GC with hydrophilic and hydrophobic GDL surfaces. The contact angles are set as 60° and 145° for the hydrophilic GDL surface and hydrophobic GDL surface, respectively.

Figures 4*a* and 5*a* show the liquid water distribution in the GC with hydrophilic GDL and hydrophobic GDL surfaces, respectively. It can be seen that the liquid water distribution is quite different. In GC with a hydrophilic GDL surface shown in Figure 4, liquid water tends to spread on the GDL surface. Due to the hydrophilic

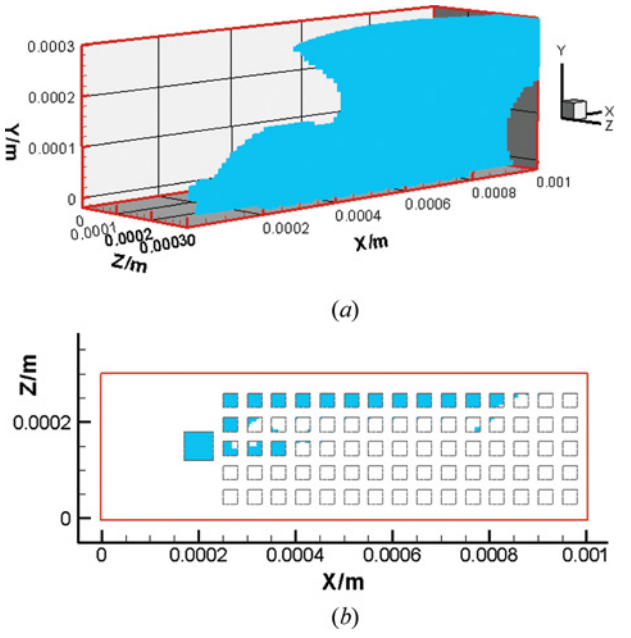

Figure 4. Liquid water distribution in GC with hydrophilic GDL at $t = 4.85$ ms (case 1, GDL contact angle = 60°). (*a*) Three-dimensional distribution, and (*b*) distribution on the GDL surface (color figure available online).

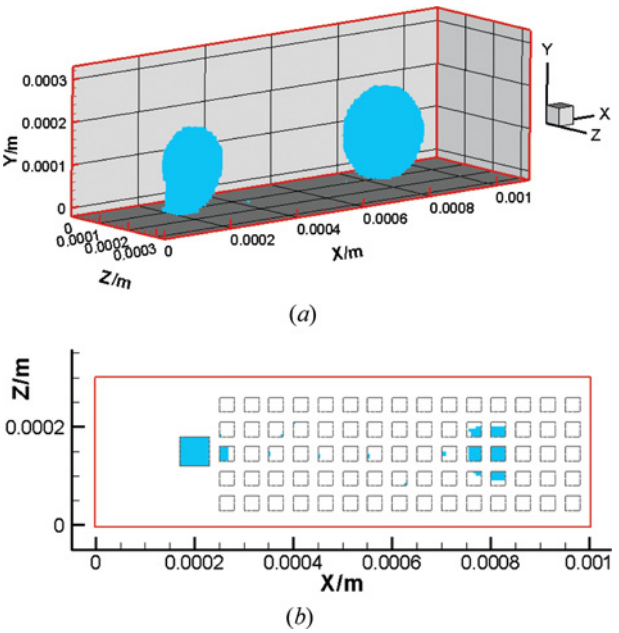

Figure 5. Liquid water distribution in GC with hydrophobic GDL at $t = 1.5$ ms (case 1, GDL contact angle = 145°). (*a*) Three-dimensional distribution and (*b*) distribution on the GDL surface (color figure available online).

surface of the top and side walls, liquid water also climbs along the side wall and covers almost half of the top wall. On the contrary, liquid water presents as water droplets and does not spread in GC due to the hydrophobic GDL in Figure 5.

Figure 4*b* shows the hydrophilic GDL surface covered by liquid water. It can be seen that many holes are filled by liquid water and thus are not available for reactant transport. For the hydrophobic GDL, only a few holes are blocked as shown in Figure 5*b*, indicating that reactants can favorably pass through the GDL. Therefore, a hydrophobic GDL surface is desirable for effective reactant transport and thus high cell performance. In the following simulations, the GDL is hydrophobic and emphasis is focused on the effects of GDL surface roughness on the behaviors of the liquid droplet.

3.2. Effects of GDL Surface Roughness

Now, we return to the subject of this study to investigate the effects of GDL surface roughness on liquid water transport in the micro GC. Five cases listed in Table 1 with different GDL surface roughness are simulated for the GDL contact angle at 125° and 145°. For all cases, liquid water dynamic behaviors in the micro GC with a hydrophobic GDL surface are similar and can be briefly described as droplet emergence (Figure 6*a*), droplet growth (Figure 6*b*), droplet detachment (Figure 6*c*), and movement of detached droplet towards the GC outlet (Figures 6*d* and 6*e*). (For more details, one can refer to reference [27]). Figure 7 shows the time evolution of liquid

water area fraction A_r at the outlet of GC for different cases with GDL contact angle. A_r is defined as A_w/A_{outlet}, where A_w is the area of water at the outlet and A_{outlet} is the total area of the outlet. Initially, A_r equals 0, implying that the detached water droplet has not arrived at the outlet. As time progresses, A_r undergoes a parabola when the liquid water is passing through the outlet, indicating that liquid water presents as droplets for all the simulation cases. Finally, A_r returns to zero when the detached droplet is completely removed out of the GC. Interestingly, Figure 7 shows that curves for cases with a rough GDL surface are different from that for case 5 with smooth GDL, implying that the GDL roughness really affects the liquid water behaviors. Besides, less time is required for a droplet to be completely removed out of the GC with a rough GDL surface compared with smooth GDL surface, indicating that rough GDL is advantageous for the removal of a water droplet. In order to better understand how GDL surface roughness affects the removal of a water droplet, forces acting on a droplet are analyzed in detail in the following section.

3.2.1. Forces acting on a water droplet. The transport process of a droplet in this study involves two stages: droplet growth stage (when the droplet still connects to the emerging pore, Figures 6*a* and 6*b* and the droplet detachment stage (the droplet has detached and moves towards the outlet of the GC, Figures 6*c*–6*e*). Obviously,

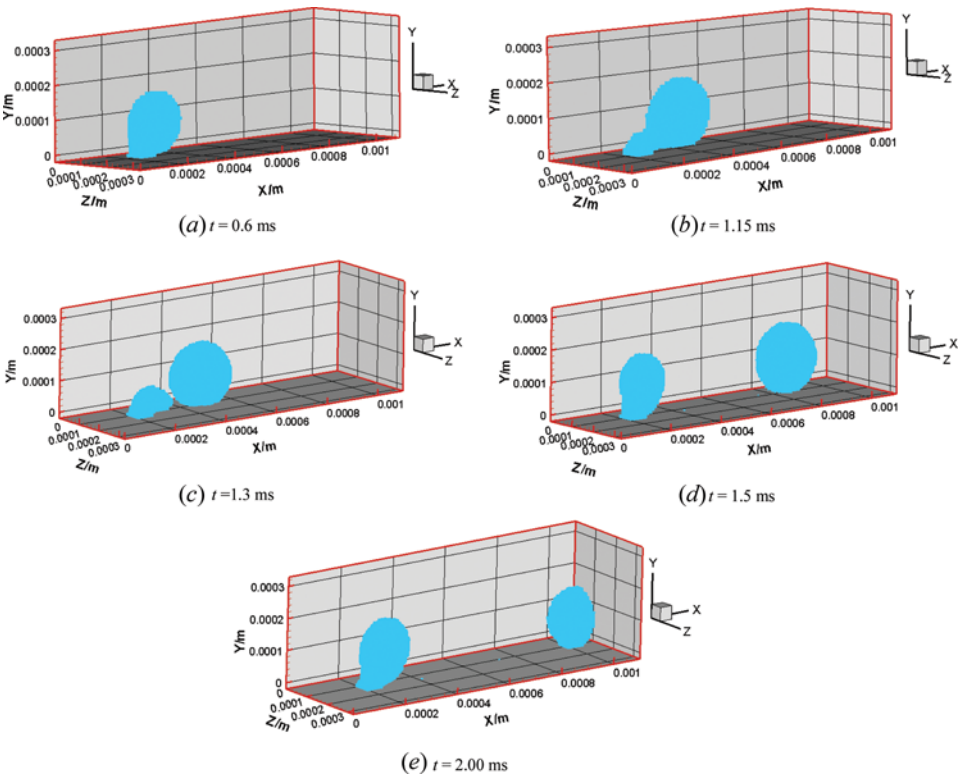

Figure 6. Time evolution of liquid water behaviors in GC (case 1, GDL contact angle = 145°) (color figure available online).

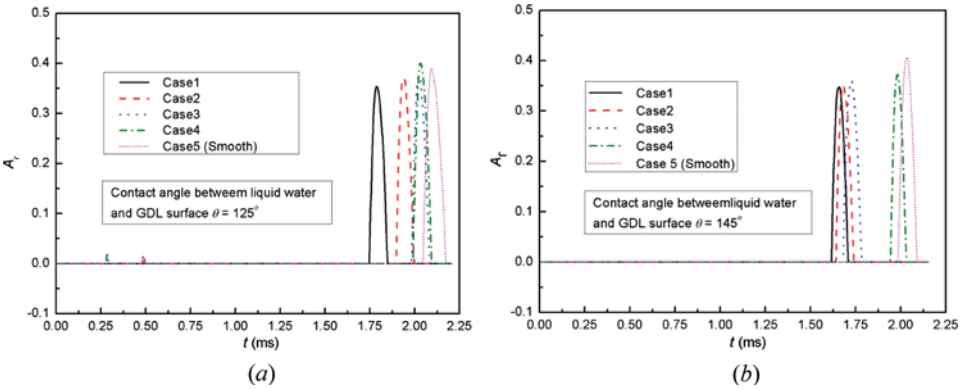

Figure 7. Time evolution of liquid water area fraction Ar at the outlet of GC for different cases. (*a*) GDL contact angle = 125° and (*b*) GDL contact angle = 145° (color figure available online).

liquid water dynamic behaviors in the two stages are combined results of several forces including shear, pressure, surface tension, gravity, buoyancy, and lift forces. In the present article, a force is called a retentive force if it holds the droplet to the GDL surface or to the emergence pore, whereas a force is called a detaching force if it tends to detach the droplet from the GDL surface or the emerging pore, or helps to remove the droplet out of the GC.

Figure 8 schematically shows a droplet suffered to air flow in GC with hydrophobic GDL. The main forces acting on a droplet when the droplet connects to the emergence pore are schematically shown in Figure 9. These forces are expressed as follows [40, 41].

Detaching forces

$$\begin{cases} x \text{ direction:} \\ F_P = 24\eta_a U_{in} H^2 R^2/b^3, \text{ pressure force} \\ F_s = 24\eta_a U_{in} H R^2/b^2, \text{ shear force} \\ y \text{ direction:} \\ F_{ad} = \pi\sigma r^2/(2R), \text{ surface tension force due to the interface pressure difference across the water - air surface} \\ F_b = \rho_a g V, \text{ buoyancy force} \\ F_l = 0.761(f\rho_a U_{in}^2/2)^{1.5}\rho_a^{-0.5} R^3/\eta_a, \text{ lift force} \end{cases} \tag{10}$$

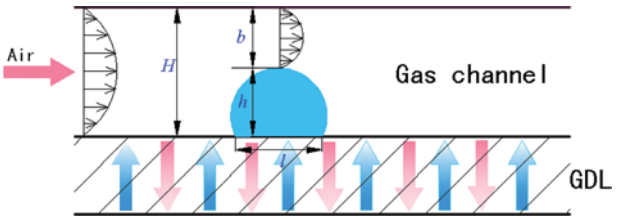

Figure 8. Schematic of a water droplet in the GC (color figure available online).

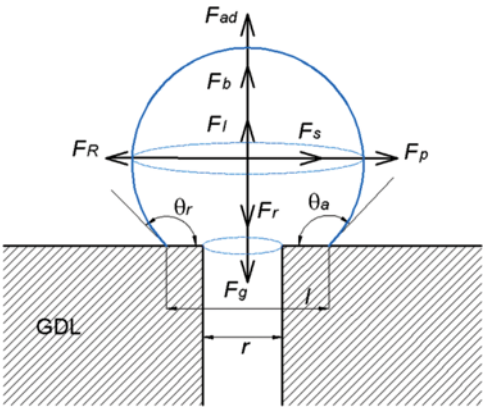

Figure 9. Forces acting on a water droplet (color figure available online).

Retentive forces

$$\begin{cases} x \text{ direction:} \\ F_R = -\sigma(\cos\theta_r - \cos\theta_a)\pi l, \text{surface force due to the water droplet deformation} \\ y \text{ direction:} \\ F_r = -2\pi\sigma r, \text{ surface force due to droplet connection to the pore} \\ F_g = -\rho_w g V, \text{ gravity force} \end{cases} \tag{11}$$

where υ_a is gas kinematic viscosity, ρ_w is density of water, ρ_a is density of air, and σ is the surface tension of water-air interface. U_{in} is the inlet air velocity, R is the radius of the water droplet, r is the radius of the emergence pore, and l is the diameter of the contact area between liquid water and the GDL surface. θ_a and θ_r are the advancing contact and the receding contact angles, respectively. H is the height of the GC, h is the height of the liquid water droplet, and b is the height between the top of the droplet and the top wall of the GC. V is the volume of the water droplet. f for a droplet in GC is defined as $16/\mathrm{Re}$, and Reynold number Re is $\mathrm{Re} = U_{in}H/\upsilon_a$.

After the water droplet detaches from the emergence pore, the bottom of the droplet contacts the solid surface instead of connecting to the emergence pore. Compared to forces acting on the water droplet during the droplet growth process, F_r vanishes as the droplet no longer connects to the emergence pore. The other forces have the same expressions as that in the growth process.

In order to roughly estimate the magnitude of the above forces, a typical condition is selected with θ_r as 115°, θ_a as 155°, and the static contact angle as 145°. Using the physical parameters previously given, forces are calculated and presented in Figure 10. It can be seen that buoyancy force and gravity force are extremely small compared to other forces. Therefore, the influences of the two forces on water droplet behaviors can be neglected.

In this study, U_{in} and H are set as constant. As the simulation is performed under isothermal condition, physical parameters ρ_a, υ_a, σ, and ρ_w also are fixed.

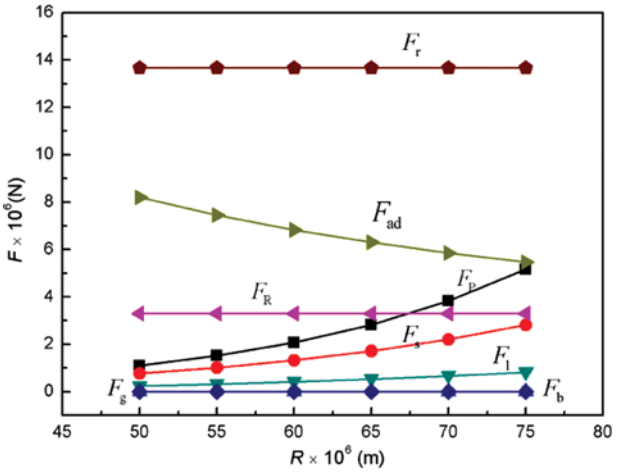

Figure 10. Forces acting on a water droplet on a smooth surface as a function of water droplet size (color figure available online).

Therefore, the alterable parameters are b, R, θ_a, θ_r, and l. Since forces acting on a droplet are directly related to these alterable parameters, effects of roughness on these parameters are explored. As the water droplet mainly moves along the flow direction, i.e., x direction, emphasis is placed on forces which are in the x direction including forces F_p, F_s, and F_R. It is worth mentioning that liquid water may be lifted from the GDL surface and moves in the y direction when the GDL contact angle exceeds certain values [27], which is beyond the scope of the present study.

3.2.2. Effects of roughness on F_r, F_p, and F_s. From the expression of F_R in Eq. (11), it can be seen that F_R is the integral around the triple-phase contact line. In order to clearly show how the GDL surface roughness affects the triple-phase contact line, liquid water distribution at $z = 0.14$ mm at different times for different cases with GDL contact angles at 125° and 145° are given in Figures 11 and 12, respectively. It can be seen from the figures that the detached droplet does not fill the holes for all cases. Instead, it moves on the top surface of the holes. Generally, a droplet on a rough surface can be described by two models: namely, the Wenzel [42] and Cassie and Baxter models [43]. The Wenzel's model assumes that liquid wets and fills the rough surface completely. On the contrary, the Cassie and Baxter model assumes that the liquid water doesn't fill the rough surface, and the interface between the liquid water and rough surface is composed of both solid and gas. As can be seen in Figures 11 and 12, liquid water sits on the top surface of the roughness elements and air is trapped in the hole which meets the Cassie and Baxter model. Thus, the detached droplet can be called a Cassie droplet. Compared to the contact area between a water droplet and smooth GDL surface, the contact area between the Cassie droplet and the rough GDL surface consists of air-water and water-solid interfaces (schematically shown in Figure 13), leading to a discontinuous triple-phase contact line. Therefore, the triple-phase contact line on the rough GDL surface is shorter than that on the smooth GDL surface, resulting in lower F_R and thus smaller retentive force. For the contact

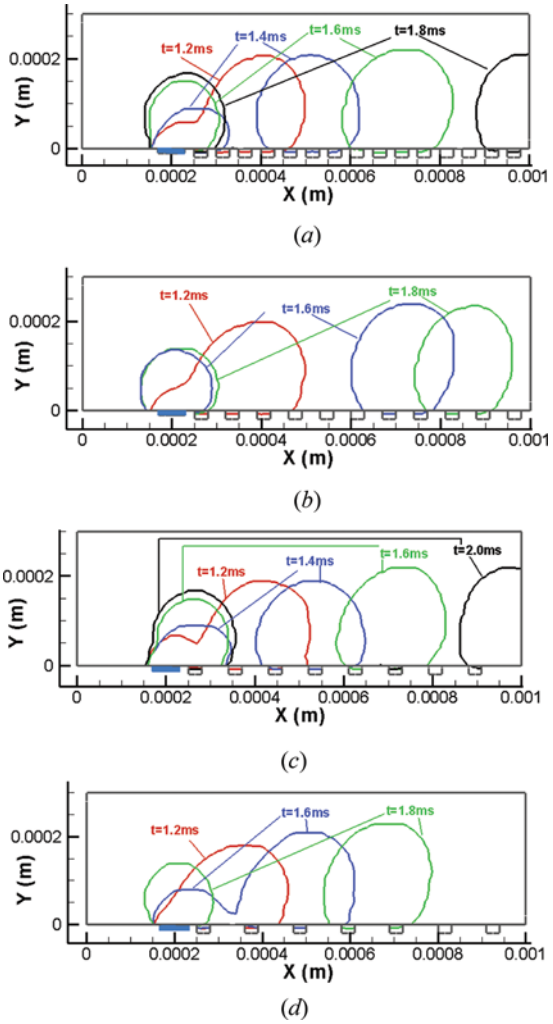

Figure 11. Liquid water distribution at $z = 0.14$ mm at different times for different cases with a GDL contact angle as 125°. (*a*) Case 1, (*b*) case 2, (*c*) case 3, and (*d*) case 4 (color figure available online).

area between a water droplet and rough GDL surface at 125° with a radius of about 70 μm (shown in Figure 13*a*), the triple-phase contact line is only about 50% of that on the smooth GDL surface, leading to considerably reduced F_R.

In order to compare the water distribution in GC with a rough GDL surface to that in GC with a smooth GDL surface, water distribution in GC with a smooth GDL surface (case 5) is also presented (as shown in Figure 14). It is clearly shown that the apparent contact angle (the appeared contact angle labeled in Figure 14*a*) on the rough GDL is higher than that on the smooth surface, although the initially given static contact angle is the same. This is expected because surface roughness can enhance the hydrophobicity of the rough surface [43]. A higher apparent contact angle gives rise to the following impacts on forces. On the one hand, for the same water droplet

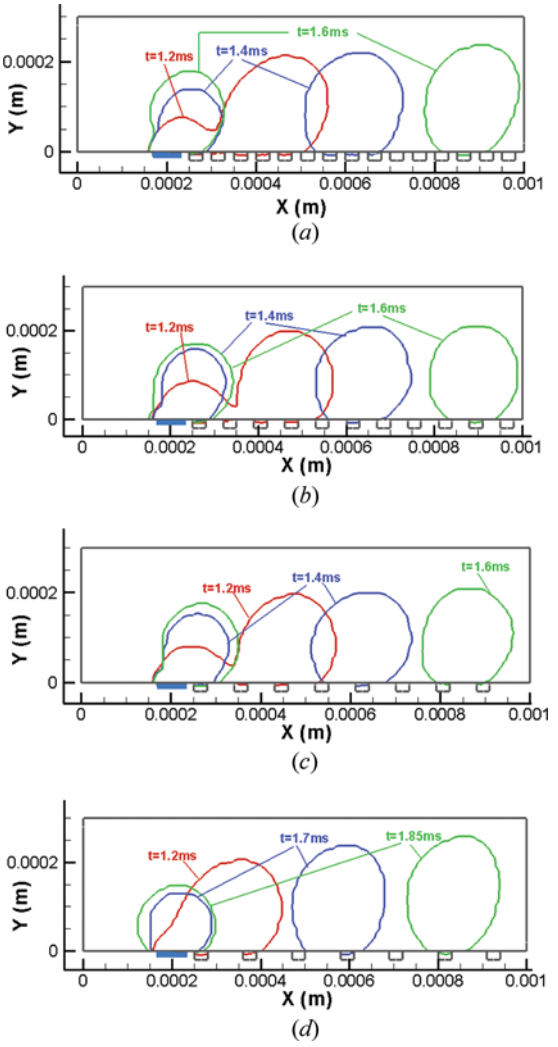

Figure 12. Liquid water distribution at $z = 0.14$ mm at different times for different cases with a GDL contact angle as 145°. (*a*) Case 1, (*b*) case 2, (*c*) case 3, and (*d*) case 4 (color figure available online).

volume a higher contact angle means a relatively taller droplet. As can be clearly seen in Figure 8, a taller droplet leads to a smaller b. According to Eq. (10), both F_p and F_s increase when b decreases, resulting in higher detaching forces. On the other hand, for the same water droplet volume a higher contact angle indicates a smaller contact area between the droplet and the GDL surface. A smaller contact area leads to a shorter triple-phase contact line and thus reduces the retentive force F_R.

3.2.3. Effects of roughness on droplet removal time. The time required for a water droplet to be removed out of the GC is a key parameter in water management in the GC. Figure 15 presents the removal time of a water droplet for different

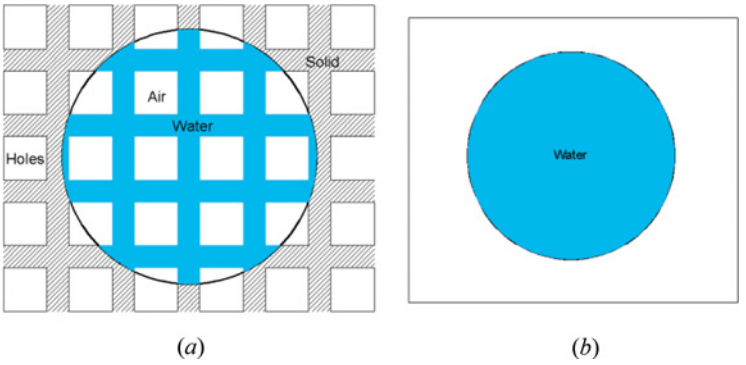

Figure 13. Schematic of the contact area between the detached droplet and GDL surface. (*a*) Rough surface, and (*b*) smooth surface. Blue: liquid water, white: air (color figure available online).

cases. Removal time of a droplet is defined as the time from the moment that a water droplet just emerges from the emergence pore to the moment that the droplet has finally been completely removed out of the GC. It can be seen that removal time in GC with rough GDL surface is shorter than that in GC with smooth GDL surface, implying quicker removal of a droplet in GC with a rough GDL surface. Obviously, the total removal time of a droplet consists of the time of the droplet growth stage (before the droplet is detached), and the time of the droplet detachment stage (after the droplet is detached). The droplet detaches if the detaching force exceeds the

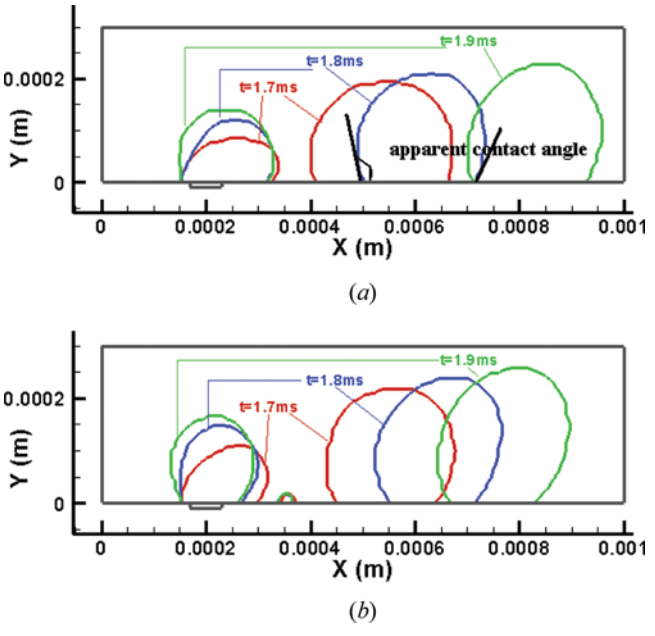

Figure 14. Liquid water distribution at $z = 0.14$ mm at different times for the smooth case. (*a*) GDL contact angle = 125°, and (*b*) GDL contact angle = 145° (color figure available online).

retentive force [44].

$$F_s + F_p > F_R \tag{12}$$

As discussed in section 3.2.2, GDL surface roughness can reduce the retentive force and increase the detaching forces. Thus, it can be concluded that detachment occurs earlier for a rough GDL based on Eq. (12), implying a shorter time of the droplet growth stage. Additionally, a rough GDL surface also reduces the time of the droplet detachment stage as the resistance force (namely F_R) decreases and the driving force (namely F_s and F_p) increases. Consequently, a rough GDL surface gives rise to quicker removal of the droplet and decreases removal time of the droplet. In reference [23], He et al. also studied the GDL surface roughness on liquid water removal time. Their simulation results, however, found out that the removal time increases as the GDL roughness increases. The contrary results obtained in the present study and in reference [23] are due to different arrangements of the roughness elements. In reference [23], roughness elements (long rectangle ribs) are prominent above the bottom GDL surface, thus hindering the liquid water movement.

3.2.4. Effects of roughness on the water coverage area on GDL surface. Another important parameter related to water management in the GC is the water coverage area on GDL surface. A smaller water coverage area on the GDL surface is desirable for reactant transport. Figure 16 shows the time evolution of the liquid water coverage ratio A_{cov} on GDL surface for different cases with contact angles at 125° and 145°. The x axis time τ has been united by the liquid removal time of each case. In Figure 16, the water coverage ratio on the GDL surface decreases as GDL surface roughness increases. This is due to two factors. On the one hand, higher surface roughness gives rise to a smaller detached droplet. On the other hand, higher surface roughness enhances the hydrophobicity of the

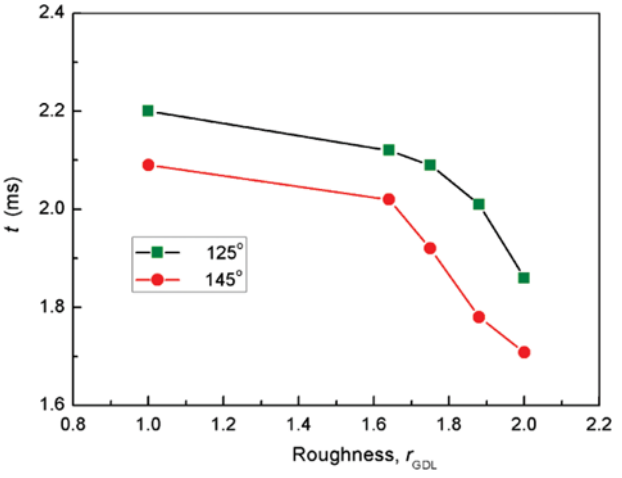

Figure 15. Removal time of the water droplet in GC for different cases (color figure available online).

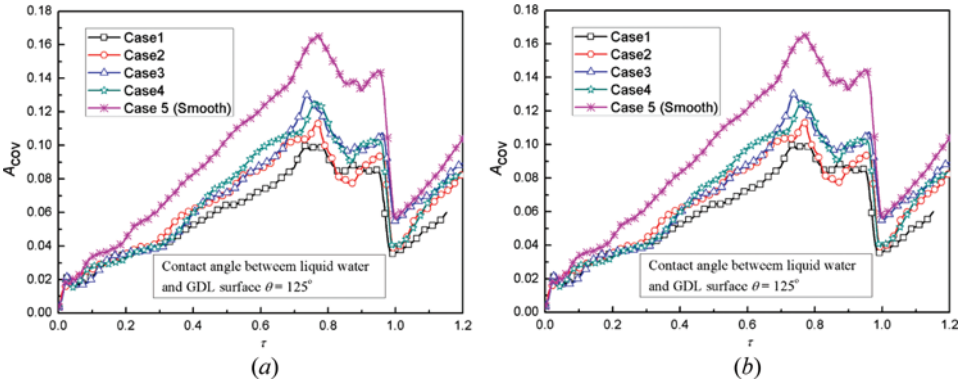

Figure 16. Time evolution of water coverage ratio on a GDL surface for different cases. (*a*) GDL contact angle = 125°, and (*b*) GDL contact angle = 145° (color figure available online).

GDL surface, and thus decreases the contact area between the droplet bottom and the GDL surface.

3.2.5. Effects of roughness on pressure drop. Pressure drop in the GC is another important parameter for fuel cell design. Compared to two-phase flow in GC with a smooth GDL surface, pressure drop in GC with a rough GDL surface will change due to two factors: one is the existence of roughness elements, and the other is the change of droplet shapes due to the surface roughness. First, for single-phase in micro-scale channels, surface roughness, even very small, will significantly influence the friction factor [45, 46]. Mala and Li [45] reported that the pressure drop in micro-channels is higher than the predictions using conventional theory. Shen et al. [46] experimentally studied single-phase convective heat transfer in rough rectangular micro-channels. They found that friction factor in the regime of higher Re is higher than the predictions using conventional theory and increases with increasing Re instead of keeping constant. Second, for two-phase flow in micro-channels, surface roughness significantly affects the flow patterns, which certainly affects the pressure drop. In this study, the surface roughness gives rise to a taller detached droplet, as discussed in section 3.2.2. Figure 17 shows the pressure drop for different cases with contact angles at 125° and 145°. The pressure drop in the figure is an averaged value by the removal time. It can be observed that pressure drop increases with the increasing GDL surface roughness, which is due to the increased roughness and the increasingly taller droplet for higher roughness.

Finally, it may be useful to note that in our paper the characteristic of the surface structure of the GDL is described by the terminology of roughness. This may not be the most accurate description of the surface character of the GDL, but it is accepted in reference [23] studying effects of GDL microstructures on liquid water behaviors, and is also widely used in other fields where liquid water movements on a surface with microstructures are considered [47–49]. From our understanding, although the GDL is something like a porous medium when the movement of a water droplet over the surface of GDL is concerned, its effects on the drop

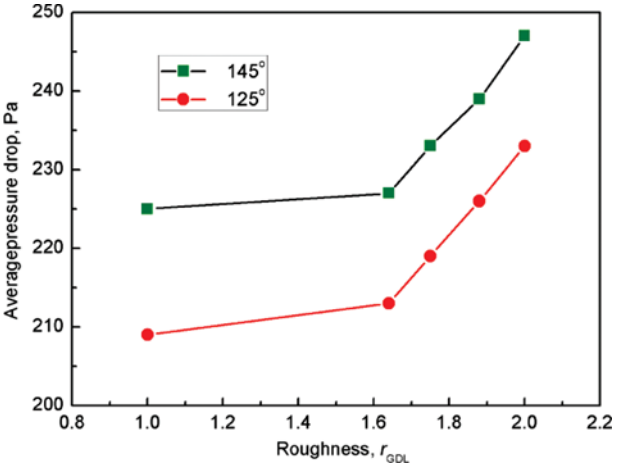

Figure 17. Averaged pressure drop for different cases (color figure available online).

movement are actually very similar to a roughened surface. In addition, the pore size and porosity adopted in our simulation (20 μm and about 0.5, respectively) are quite close to the typical values of a carbon paper GDL (pore size 1-100 μm and porosity about 0.8, which will be reduced if a hydrophobic agent PTFE is added). The surface structure reconstructed based on such dimensions (Figure 2) may be regarded as a surface with micro-roughness.

4. CONCLUSION

In this study, liquid water transport in a micro GC with a rough GDL surface is investigated. Effects of GDL surface roughness on forces acting on a water droplet are carefully explored. Effects of GDL surface roughness on liquid water removal time, liquid water coverage area ratio on GDL surface, and pressure drop in the GC also are studied. The main conclusions are derived as follows.

- A Cassie droplet is inclined to form in the micro GC with rough and hydrophobic GDL surfaces. The GDL surfaces roughness increases the apparent contact angle between the droplet and GDL surface, and decreases the triple-phase contact line. Thus, the GDL surface roughness leads to lower retentive forces and higher detaching forces acting on the water droplet.
- The GDL surface roughness accelerates the removal of a droplet. The higher the roughness is, the less the removal time.
- The GDL surface roughness reduces the water coverage ratio on the GDL surface because the roughness enhances the surface hydrophobicity. The rougher the surface is, the less the GDL surface is covered by water.
- The GDL surface roughness increases the pressure drop in the GC. The rougher the surface is, the higher the pressure drop is.

REFERENCES

1. H. Li, Y. Tang, Z. Wang, Z. Shi, S. Wu, D. Song, J. Zhang, K. Fatih, J. Zhang, H. Wang, Z. Liu, R. Abouatallah, and A. Mazza, A Review of Water Flooding Issues in the Proton Exchange Membrane Fuel Cell, *J. of Power Sources*, vol. 178, no. 1, pp. 103–117, 2008.
2. A. Bazylak, Liquid Water Visualization in PEM Fuel Cells: A Review, *Int. J. of Hydrogen Energy*, vol. 34, no. 9, pp. 3845–3857, 2009.
3. R. Anderson, L. Zhang, Y. Ding, M. Blanco, X. Bi, and D. P. Wilkinson, A Critical Review of Two-Phase Flow in Gas Flow Channels of Proton Exchange Membrane Fuel Cells, *J. of Power Sources*, vol. 195, no. 15, pp. 4531–4553, 2010.
4. F. Y. Zhang, X. G. Yang, and C. Y. Wang, Liquid Water Removal from a Polymer Electrolyte Fuel Cell, *J. of the Electrochemical Society*, vol. 153, no. 2, pp. A225–A232, 2006.
5. J. P. Owejan, T. A. Trabold, D. L. Jacobson, D. R. Baker, D. S. Hussey, and M. Arif, In Situ Investigation of Water Transport in an Operating PEM Fuel Cell using Neutron Radiography: Part 2—Transient Water Accumulation in an Interdigitated Cathode Flow Field, *Int. J. of Heat and Mass Transfer*, vol. 49, no. 25–26, pp. 4721–4731, 2006.
6. T. Ous and C. Arcoumanis, Visualisation of Water Accumulation in the Flow Channels of PEMFC under Various Operating Conditions, *J. of Power Sources*, vol. 187, no. 1, pp. 182–189, 2009.
7. N. Pekula, K. Heller, P. A. Chuang, A. Turhan, M. M. Mench, J. S. Brenizer, and K. Ünlü, Study of Water Distribution and Transport in a Polymer Electrolyte Fuel Cell using Neutron Imaging, *Nuclear Instruments and Methods in Physics Research Section A: Accelerators, Spectrometers, Detectors and Associated Equipment*, vol. 542, no. 1–3, pp. 134–141, 2005.
8. D. Spernjak, A. K. Prasad, and S. G. Advani, In Situ Comparison of Water Content, and Dynamics in Parallel, Single-Serpentine, and Interdigitated Flow Fields of Polymer Electrolyte Membrane Fuel Cells, *J. of Power Sources*, vol. 195, no. 11, pp. 3553–3568, 2011.
9. J. P. Owejan, T. A. Trabold, D. L. Jacobson, M. Arif, and S. G. Kandlikar, Effects of Flow Field and Diffusion Layer Properties on Water Accumulation in a PEM Fuel Cell, *Int. J. of Hydrogen Energy*, vol. 32, no. 17, pp. 4489–4502, 2007.
10. A. Turhan, K. Heller, J. S. Brenizer, and M. M. Mench, Passive Control of Liquid Water Storage and Distribution in a PEFC Through Flow-Field Design, *J. of Power Sources*, vol. 180, no. 2, pp. 773–783, 2008.
11. A. Turhan, S. Kim, M. Hatzell, and M. M. Mench, Impact of Channel Wall Hydrophobicity on Through-Plane Water Distribution and Flooding Behavior in a Polymer Electrolyte Fuel Cell, *Electrochimica Acta*, vol. 55, no. 8, 2734–2745, 2010.
12. Z. H. Wang, C. Y. Wang, and K. S. Chen, Two-Phase Flow and Transport in the Air Cathode of Proton Exchange Membrane Fuel Cells, *J. of Power Sources*, vol. 94, no. 1, pp. 40–50, 2001.
13. L. You and H. Liu, A Two-Phase Flow and Transport Model for the Cathode of PEM Fuel Cells, *Int. J. of Heat and Mass Transfer*, vol. 45, no. 11, pp. 2277–2287, 2002.
14. T. Berning and N. Djilali, Three-Dimensional Computational Analysis of Transport Phenomena in a PEM Fuel Cell–a Parametric Study, *J. of Power Sources*, vol. 124, no. 2, pp. 440–452, 2003.
15. V. Gurau, J. A. Mann, and T. A. Zawodzinski, Two-Phase Transport in PEM Fule Cell Cathodes, *J. of Fuel Cell Sicence and Tech.*, vol. 5, (021009–1-021009–12), 2008.
16. V. Gurau and J. A. Mann, Effect of Interfacial Phenomena at the Gas Diffusion Layer-Channel Interface on the Water Evolution in a PEMFC, *J. of the Electrochemical Society*, vol. 157, no. 4, pp. B512–B521, 2010.

17. P. Quan, B. Zhou, A. Sobiesiak, and Z. Liu, Water Behavior in Serpentine Micro-Channel for Proton Exchange Membrane Fuel Cell Cathode, *J. of Power Sources*, vol. 152, pp. 131–145, 2005.
18. K. Jiao, B. Zhou, and P. Quan, Liquid Water Transport in Straight Micro-Parallel-Channels with Manifolds for PEM Fuel Cell Cathode, *J. of Power Sources*, vol. 157, no. 1, pp. 226–243, 2006.
19. Y. H. Cai, J. Hu, H. P. Ma, B. L. Yi, and H. M. Zhang, Effects of Hydrophilic/Hydrophobic Properties on the Water Behavior in the Micro-Channels of a Proton Exchange Membrane Fuel Cell, *J. of Power Sources*, vol. 161, no. 2, pp. 843–848, 2006.
20. Z. Zhan, J. Xiao, M. Pan, and R. Yuan, Characteristics of Droplet and Film Water Motion in the Flow Channels of Polymer Electrolyte Membrane Fuel Cells, *J. of Power Sources*, vol. 160, no. 1, pp. 1–9, 2006.
21. K. Jiao, B. Zhou, and P. Quan, Liquid Water Transport in Parallel Serpentine Channels with Manifolds on Cathode Side of a PEM Fuel Cell Stack, *J. of Power Sources*, vol. 154, no. 1, pp. 124–137, 2006.
22. S. Ebrahim and M. Shila, Deformation of a Droplet in a Channel Flow, *J. of Fuel Cell Sci. and Techn.*, vol. 5, no. 4, pp. 041008, 2008.
23. G. He, Y. Yamazaki, and A. Abudula, The Effect of Wall Roughness on the Liquid Removal in Micro-Channels Related to a Proton Exchange Membrane Fuel Cell (PEMFC), *J. of Power Sources*, vol. 195, no. 6, pp. 1561–1568, 2010.
24. N. Akhtar and P. J. A. M. Kerkhof, Dynamic Behavior of Liquid Water Transport in a Tapered Channel of a Proton Exchange Membrane Fuel Cell Cathode, *Int. J. of Hydrogen Energy*, vol. 36, no. 4, pp. 3076–3086, 2011.
25. A. Theodorakakos, T. Ous, M. Gavaises, J. M. Nouri, N. Nikolopoulos, and H. Yanagihara, Dynamics of Water Droplets Detached from Porous Surfaces of Relevance to PEM Fuel Cells, *J. of Colloid and Interface Sci.*, vol. 300, no. 2, pp. 673–687, 2006.
26. X. Zhu, P. C. Sui, and N. Djilali, Dynamic Behaviour of Liquid Water Emerging from a GDL Pore into a PEMFC Gas Flow Channel, *J. of Power Sources*, vol. 172, no. 1, pp. 287–295, 2007.
27. X. Zhu, P. C. Sui, and N. Djilali, Three-Dimensional Numerical Simulations of Water Droplet Dynamics in a PEMFC Gas Channel, *J. of Power Sources*, vol. 181, no. 1, pp. 101–115, 2008.
28. X. Zhu, Q. Liao, P. C. Sui, and N. Djilali, Numerical Investigation of Water Droplet Dynamics in a Low-Temperature Fuel Cell Microchannel: Effect Of Channel Geometry, *J. of Power Sources*, vol. 195, no. 3, pp. 801–812, 2010.
29. Y. Ding, H. T. Bi, and D. P. Wilkinson, Three-Dimensional Numerical Simulation of Water Droplet Emerging from a Gas Diffusion Layer Surface in Micro-Channels, *J. of Power Sources*, vol. 195, no. 21, pp. 7278–7288, 2010.
30. A. D. Le, B. Zhou, H.-R. Shiu, C.-I. Lee, and W.-C. Chang, Numerical Simulation and Experimental Validation of Liquid Water Behaviors in a Proton Exchange Membrane Fuel Cell Cathode with Serpentine Channels, *J. of Power Sources*, vol. 195, no. 21, pp. 7302–7315, 2010.
31. K. Jiao and B. Zhou, Innovative Gas Diffusion Layers and Their Water Removal Characteristics in PEM Fuel Cell Cathode, *J. of Power Sources*, vol. 169, no. 2, pp. 296–314, 2007.
32. K. Jiao and B. Zhou, Effects of Electrode Wettabilities on Liquid Water Behaviours in PEM Fuel Cell Cathode, *J. of Power Sources*, vol. 175, no. 1, pp. 106–119, 2008.
33. A. D. Le and B. Zhou, A General Model of Proton Exchange Membrane Fuel Cell, *J. of Power Sources*, vol. 182, no. 1, pp. 197–222, 2008.

34. A. D. Le and B. Zhou, A Generalized Numerical Model for Liquid Water in a Proton Exchange Membrane Fuel Cell with Interdigitated Design, *J. of Power Sources*, vol. 193, no. 2, pp. 665–683, 2009.
35. D. L. Youngs, *Numerical Methods for Fluid Dynamics*, Academic Press: New York, 1982.
36. Fluent 6.3 User's Guide, Fluent Inc., 2006.
37. J. U. Brackbill, D. B. Kothe, and C. Zemach, A Continuum Method for Modeling Surface Tension, *J. of Computational Physics*, vol. 100, no. 2, pp. 335–354, 1992.
38. P. C. Sui and N. Djilali, Analysis of Water Transport in Proton Exchange Membranes Using a Phenomenological Model, *ASME J. of Fuel Cell Sci. and Techn.*, vol. 2, no. 3, pp. 149–155, 2005.
39. A. Bazylak, D. Sinton, Z. S. Liu, and N. Djilali, Effect of Compression on Liquid Water Transport and Microstructure of PEMFC Gas Diffusion Layers, *J. of Power Sources*, vol. 163, no. 2, pp. 784–792, 2007.
40. Z. Wang and S. C. Wang, Effect of Continuous Phase Viscosity on Membrane Emulsification, *Chin. J. Chem. Eng.*, vol. 8, pp. 108–112, 2002.
41. G. D. Luca, A. Sindona, L. Giorno et al. Quantitative Analysis of Coupling Effects in Cross-Flow Membrane Emulsification, *J. Membr. Sci.*, vol. 29, pp. 199–209, 2004.
42. R. N. Wenzel, Resistance of Solid Surface to Wetting by Water, *Industrial and Engi. chem.*, vol. 28, pp. 988–994, 1936.
43. A. B. D. Cassie and S. Baxter, Wettability of Porous Surfaces, *Trans. of the Faraday Society*, vol. 40, pp. 546–551, 1994.
44. E. C. Kumbur, K. V. Sharp, and M. M. Mench, Liquid Droplet Behavior and Instability in a Polymer Electrolyte Fuel Cell Flow Channel, *J. of Power Sources*, vol. 161, no. 1, pp. 333–345, 2006.
45. G. Mohiuddin Mala and D. Li, Flow Characteristics of Water in Microtubes, *Int. J. of Heat and Fluid Flow*, vol. 20, no. 2, pp. 142–148, 1999.
46. S. Shen, J. L. Xu, J. J. Zhou, and Y. Chen, Flow and Heat Transfer in Microchannels with Rough Wall Surface, *Energy Conversion and Management*, vol. 47, no. 11–12, pp. 1311–1325, 2006.
47. Z. Yoshimitsu, A. Nakajima, T. Watanabe, and K. Hashimoto, Effects of Surface Structure on the Hydrophobicity and Sliding Behavior of Water Droplets, *Langmuir*, vol. 18, no. 15, pp. 5818–5822, 2002.
48. B. He, N. A. Patankar, and J. Lee, Multiple Equilibrium Droplet Shapes and Design Criterion for Rough Hydrophobic Surfaces, *Langmuir*, vol. 19, no. 12, pp. 4999–5003, 2003.
49. C. Sun, X.-W. Zhao, Y.-H. Han, and Z.-Z. Gu, Control of Water Droplet Motion by Alteration of Roughness Gradient on Silicon Wafer by Laser Surface Treatment, *Thin Solid Films*, vol. 516, no. 12, pp. 4059–4063, 2008.